Molecular Crystals and Liquid Crystals

Publication details, including instructions for authors and subscription information:
http://www.tandfonline.com/loi/gmcl20

Lattice Boltzmann Simulations of Cholesteric Liquid Crystals: Permeative Flows, Doubly Twisted Textures and Cubic Blue Phases

D. Marenduzzo [a] , A. Dupuis [b] , J. M. Yeomans [b] & E. Orlandini [c]

[a] The Rudolf Peierls Centre for Theoretical Physics, Oxford, England, and Mathematics Institute, University of Warwick, Coventry, England

[b] The Rudolf Peierls Centre for Theoretical Physics, Oxford, England

[c] INFM, Dipartimento di Fisica, Universita' di Padova, Padova, Italy

Version of record first published: 31 Aug 2006

To cite this article: D. Marenduzzo, A. Dupuis, J. M. Yeomans & E. Orlandini (2005): Lattice Boltzmann Simulations of Cholesteric Liquid Crystals: Permeative Flows, Doubly Twisted Textures and Cubic Blue Phases, Molecular Crystals and Liquid Crystals, 435:1, 185/[845]-198/[858]

To link to this article: http://dx.doi.org/10.1080/15421400590956658

Mol. Cryst. Liq. Cryst., Vol. 435, pp. 185/[845]–198/[858], 2005

ISSN: 1542-1406 print/1563-5287 online
DOI: 10.1080/15421400590956658

Taylor & Francis
Taylor & Francis Group

Lattice Boltzmann Simulations of Cholesteric Liquid Crystals: Permeative Flows, Doubly Twisted Textures and Cubic Blue Phases

D. Marenduzzo
The Rudolf Peierls Centre for Theoretical Physics, Oxford, England and Mathematics Institute, University of Warwick, Coventry, England

A. Dupuis
J. M. Yeomans
The Rudolf Peierls Centre for Theoretical Physics, Oxford, England

E. Orlandini
INFM, Dipartimento di Fisica, Universita' di Padova, Padova, Italy

We present a lattice Boltzmann algorithm to solve the Beris-Edwards equations of motion for a cholesteric liquid crystal. We use our algorithm to investigate permeative flow. We find that, for helices pinned at the boundary, a small body force leads to a huge viscosity increase whereas larger ones induce no increase. This shear thinning is in agreement with experiments. If, instead, the helix lies perpendicular to the plates, there is almost no viscosity increase. For strong forcing, we identify a flow-induced double twist in the director field. We compare this texture with the static double twist of cubic blue phases.

Keywords: blue phases; cholesterics; double twist; hydrodynamics; permeation

I. INTRODUCTION

Liquid crystals are typically composed of highly anisotropic molecules. They are viscoelastic materials; some of their properties are typical of a liquid while others are usually associated with solids. As liquids, they can flow and they exhibit a viscous response to an applied stress. However, liquid crystals also possess long-range, orientational order

Address correspondence to Davide Marenduzzo, Mathematics Institute, University of Warwick Gibbett Hill Road, Coventry CV4 7AL, England. E-mail: davide@maths.warwick.ac.uk

[1,2] which results from the entropic advantage of aligning the constituent molecules. The long-range, orientational order is usefully described by the director field $\vec{n}$, the coarse-grained, average, molecular orientation. In a cholesteric or chiral nematic liquid crystal $\vec{n}$ has a natural twist deformation along an axis perpendicular to the molecules [1,2]. Examples of cholesteric liquid crystals are DNA molecules in solution [3,4], colloidal suspensions of bacteriophages [5], and solutions of nematic mixtures with chiral dopants [6] which are widely used in display devices.

Cholesteric liquid crystals present a number of very intriguing properties. Even the understanding of their equilibrium phase diagram required the development of complicated theories and still presents open challenges. When a liquid crystal is cooled down from the isotropic into the cholesteric phase, instead of a direct transition into a helical configuration, the system passes through a series of first order phase transitions – all intervening in a narrow temperature range of roughly $1K$ [7,8]. These intermediate phases are known as blue phases (blue phase I, II and III are documented) and are of technological relevance as well [9,10]. Blue phase I and II (BP I and BP II) display a cubic symmetry, while blue phase III (BP III) has an amorphous nature. Identifying the structure of cubic blue phases presented a considerable theoretical challenge [7,11–13]. The key to this issue is the realisation that blue phases are obtained by patching together distinct regions in which the director has a doubly twisted texture. This procedure cannot be done without creating defects, and indeed a blue phase can be imagined as a periodic network of disclination lines.

Cholesteric liquid crystals display puzzling and strongly non-Newtonian viscous properties in a hydrodynamic flow as well. When a cholesteric is subjected to a slow imposed flow in the direction of the helix axis, its viscosity can increase enormously (by a factor $\sim 10^5$) when the isotropic to cholesteric transition is reached [14–18]. This phenomenon is often referred to (mainly for historic reasons) as *permeation*. The viscosity then dropped to values close to those of a normal liquid as the pressure difference imposing the flow was increased.

An explanation of permeation was first given by Helfrich [14]. If the director orientation is fixed in space, due for example to anchoring effects at the wall, any flow along the helix must be linked with a rotation of the molecules. This leads to an energy dissipation far larger than that due to the usual molecular friction and hence a much enhanced viscosity [14]. After Helfrich's paper, a few other authors generalised and extended these ideas [1,2,19]. These analytic calculations all assume small forcing, so that the director field is not

deformed by the helix. There is an interesting suggestion in an early paper by Prost *et al.* [20] that an increase in forcing might stabilise a modulation in the director field in a direction perpendicular to the flow.

So even if Helfrich's explanation of permeation is widely accepted, many questions still remain at the theoretical level. It is interesting for example to ask whether distortions in the director field, induced by the flow, alter the permeation. Also, does permeation persist beyond the regime of low forcing and what replaces it for larger forcing? Finally, how does the theoretically calculated apparent viscosity depend on the forcing or shear rate?

Here, in order to obtain a more complete theoretical understanding of these phenomena, we set up a numerical method – based on a lattice Boltzmann algorithm – which can solve the Beris-Edwards hydrodynamic equations of motion of a cholesteric liquid crystal. We apply our algorithm to study permeative flow (helical axis parallel to the flow direction). We find that if the helix is pinned at the boundaries, there is a huge viscosity increase when the forcing is small enough. The cholesteric layers are bent into chevrons. For very large forcing, the initial structure is destroyed and the viscosity drops to values close of those of an isotropic fluid. Before this happens, we identify an intriguing structure in which the chevrons are replaced by a doubly twisted texture near the center of the channel. We finally compare the *dynamic* double twist found here with the *static* doubly twist usually associated with blue phases. To this aim, we equilibrate two configurations, corresponding to BP I and BP II respectively, again by means of a solution of the Beris-Edwards equations of motion.

This paper is organised as follows. In section II, we summarise the Beris-Edwards equations of motion which apply in the case of cholesterics, and then we introduce the lattice Boltzmann algorithm used to solve them. In section III, we first report the results on the viscous properties of a cholesteric subjected to permeative flow, and then we compare the dynamic doubly twisted texture with the textures (and disclination line structures) of BP I and BP II. Section IV contains our conclusions.

II. MODELS AND METHODS

A. Beris-Edwards Equations of Motion

We consider the formulation of liquid crystal hydrodynamics given by Beris and Edwards [21], generalised for cholesteric liquid crystals.

The equations of motion are written in terms of a tensor order parameter $\mathbf{Q}$ which is related to the direction of individual molecules, $\hat{n}$, by $Q_{\alpha\beta} = \langle \hat{n}_\alpha \hat{n}_\beta - \frac{1}{3}\delta_{\alpha\beta} \rangle$ where the angular brackets denote a coarse-grained average and the Greek indices label the Cartesian components of $\mathbf{Q}$. The tensor $\mathbf{Q}$ is traceless and symmetric. Its largest eigenvalue, $\frac{2}{3}q$, $0 < q < 1$, describes the magnitude of the order.

The equilibrium properties of the liquid crystal are described by a Landau-de Gennes free energy density. This comprises a bulk term (summation over repeated indices is implied hereafter),

$$\frac{A_0}{2}\left(1 - \frac{\gamma}{3}\right)Q_{\alpha\beta}^2 - \frac{A_0\gamma}{3}Q_{\alpha\beta}Q_{\beta\gamma}Q_{\gamma\alpha} + \frac{A_0\gamma}{4}(Q_{\alpha\beta}^2)^2, \tag{1}$$

and a distortion term, which we take as in [1,7] to be

$$\frac{K}{2}\left[(\partial_\beta Q_{\alpha\beta})^2 + \left(\epsilon_{\alpha\zeta\delta}\partial_\zeta Q_{\delta\beta} + \frac{4\pi}{p}Q_{\alpha\beta}\right)^2\right], \tag{2}$$

where K is an elastic constant and p is the helix pitch. The tensor $\epsilon_{\alpha\zeta\delta}$ is the Levi-Civita antisymmetric third-rank tensor, A_0 is a constant and γ controls the magnitude of order.

The anchoring of the director field on the boundary surfaces to a chosen director $\hat{n}^0$ is ensured by adding the surface term

$$f_s = \frac{1}{2}W_0(Q_{\alpha\beta} - Q_{\alpha\beta}^0)^2 \tag{3}$$

$$Q_{\alpha\beta}^0 = S_0(n_\alpha^0 n_\beta^0 - \delta_{\alpha\beta}/3) \tag{4}$$

The parameter W_0 controls the strength of the anchoring, while S_0 determines the degree of the surface order. If the surface order is equal to the bulk order, S_0 should be taken equal to q.

The equation of motion for $\mathbf{Q}$ is [21]

$$(\partial_t + \vec{u}\cdot\nabla)\mathbf{Q} - \mathbf{S}(\mathbf{W},\mathbf{Q}) = \Gamma\mathbf{H} \tag{5}$$

where Γ is a collective rotational diffusion constant and $\vec{u}$ is the fluid velocity. The tensor $\mathbf{S}$ is explicitly

$$\begin{aligned}\mathbf{S}(\mathbf{W},\mathbf{Q}) = {} & (\xi\mathbf{D} + \Omega)(\mathbf{Q} + \mathbf{I}/3) + (\mathbf{Q} + \mathbf{I}/3)(\xi\mathbf{D} - \Omega) \\ & - 2\xi(\mathbf{Q} + \mathbf{I}/3)\mathrm{Tr}(\mathbf{Q}\mathbf{W})\end{aligned} \tag{6}$$

where Tr denotes the tensorial trace, while $\mathbf{D} = (\mathbf{W} + \mathbf{W}^T)/2$ and $\Omega = (\mathbf{W} - \mathbf{W}^T)/2$ are the symmetric part and the anti-symmetric part respectively of the velocity gradient tensor $W_{\alpha\beta} = \partial_\beta u_\alpha$. The constant ξ depends on the molecular details of a given liquid crystal and

determines whether the liquid crystal is flow aligning or tumbling [1]. We will restrict to flow aligning liquid crystals in the results reported in section III. What reported here refers to flow aligning liquid crystals. The molecular field **H** which provides the driving motion is related to the functional derivative of the free energy, $\mathcal{F}$:

$$\mathbf{H} = -\frac{\delta \mathcal{F}}{\delta \mathbf{Q}} + (\mathbf{I}/3)\mathrm{Tr}\frac{\delta \mathcal{F}}{\delta \mathbf{Q}}. \tag{7}$$

The fluid velocity, $\vec{u}$, obeys the continuity equation and the Navier-Stokes equation,

$$\begin{aligned}\rho(\partial_t + u_\beta \partial_\beta)u_\alpha = \partial_\beta(\Pi_{\alpha\beta}) + \eta\partial_\beta(\partial_\alpha u_\beta + \partial_\beta u_\alpha \\ + (1 - 3\partial_\rho P_0)\partial_\gamma u_\gamma \delta_{\alpha\beta}),\end{aligned} \tag{8}$$

where ρ is the fluid density and η is an isotropic viscosity. The stress tensor $\Pi_{\alpha\beta}$ necessary to describe liquid crystal hydrodynamics is:

$$\begin{aligned}\Pi_{\alpha\beta} = &-P_0\delta_{\alpha\beta} + 2\xi(Q_{\alpha\beta} + \frac{1}{3}\delta_{\alpha\beta})Q_{\gamma\epsilon}H_{\gamma\epsilon} \\ &- \xi H_{\alpha\gamma}(Q_{\gamma\beta} + \frac{1}{3}\delta_{\gamma\beta}) - \xi(Q_{\alpha\gamma} + \frac{1}{3}\delta_{\alpha\gamma})H_{\gamma\beta} \\ &- \partial_\alpha Q_{\gamma\nu}\frac{\delta \mathcal{F}}{\delta \partial_\beta Q_{\gamma\nu}} + Q_{\alpha\gamma}H_{\gamma\beta} - H_{\alpha\gamma}Q_{\gamma\beta}.\end{aligned} \tag{9}$$

P_0 is a constant in the simulations reported here.

The differential equations Eq. (5) and Eq. (8) are coupled. Unless the flow field is zero ($\vec{u} = 0$) the dynamics given by Eq. (5) are not purely relaxational. Conversely, the order parameter field affects the dynamics of the flow field through the stress tensor. This is called the back-flow coupling.

B. Lattice Boltzmann Algorithm

To solve these equations we use a lattice Boltzmann algorithm, originally introduced in Refs. [22,23] for nematic liquid crystals. Usually lattice Boltzmann algorithms, describing the Navier-Stokes equations of a simple fluid, are defined in terms of a single set of partial distribution functions, the scalars $f_i(\vec{x})$, that sum on each lattice site $\vec{x}$ to give the density [24]. For liquid crystal hydrodynamics, this must be supplemented by a second set, the symmetric traceless tensors $\mathbf{G}_i(\vec{x})$, that are related to the tensor order parameter **Q**. Each f_i, $\mathbf{G}_i$ is associated with a lattice vector $\vec{e}_i$. We choose a 15-velocity model on the cubic

lattice with lattice vectors:

$$\vec{e}_i^{(0)} = (0,0,0) \tag{10}$$

$$\vec{e}_i^{(1)} = (\pm 1,0,0),(0,\pm 1,0),(0,0,\pm 1) \tag{11}$$

$$\vec{e}_i^{(2)} = (\pm 1,\pm 1,\pm 1). \tag{12}$$

The indices, i, are ordered so that $i=0$ corresponds to $\vec{e}_i^{(0)}$, $i=1,\ldots,6$ correspond to the $\vec{e}_i^{(1)}$ set and $i=7,14$ to the $\vec{e}_i^{(2)}$.

Physical variables are defined as moments of the distribution function:

$$\rho = \sum_i f_i, \qquad \rho u_\alpha = \sum_i f_i e_{i\alpha}, \qquad \mathbf{Q} = \sum_i \mathbf{G}_i. \tag{13}$$

The distribution functions evolve in a time step Δt according to

$$\begin{aligned} f_i(\vec{x}+\vec{e}_i\Delta t, t+\Delta t) - f_i(\vec{x},t) = & \frac{\Delta t}{2}\Big[\mathcal{C}_{fi}(\vec{x},t,\{f_i\}) + \mathcal{C}_{fi}(\vec{x}+\vec{e}_i\Delta t, t \\ & + \Delta t, \{f_i^*\})\Big]\mathbf{G}_i(\vec{x}+\vec{e}_i\Delta t, t+\Delta t) - \mathbf{G}_i(\vec{x},t) \qquad (14) \\ = & \frac{\Delta t}{2}\Big[\mathcal{C}_{\mathbf{G}i}(\vec{x},t,\{\mathbf{G}_i\}) + \mathcal{C}_{\mathbf{G}i}(\vec{x}+\vec{e}_i\Delta t, t \\ & + \Delta t, \{\mathbf{G}_i^*\})\Big] \qquad (15) \end{aligned}$$

This represents free streaming with velocity $\vec{e}_i$ followed by a collision step which allows the distribution to relax towards their equilibrium. f_i^* and $\mathbf{G}_i^*$ are first order approximations to $f_i(\vec{x}+\vec{e}_i dt, t+dt)$ and $\mathbf{G}_i(\vec{x}+\vec{e}_i dt, t+dt)$ respectively [23].

The collision operators are taken to have the form of a single relaxation time Boltzmann equation, together with a forcing term

$$\mathcal{C}_{fi}(\vec{x},t,\{f_i\}) = -\frac{1}{\tau_f}\left(f_i(\vec{x},t) - f_i^{eq}(\vec{x},t,\{f_i\})\right) + p_i(\vec{x},t,\{f_i\}), \tag{16}$$

$$\mathcal{C}_{\mathbf{G}i}(\vec{x},t,\{\mathbf{G}_i\}) = -\frac{1}{\tau_{\mathbf{G}}}\left(\mathbf{G}_i(\vec{x},t) - \mathbf{G}_i^{eq}(\vec{x},t,\{\mathbf{G}_i\})\right) + \mathbf{M}_i(\vec{x},t,\{\mathbf{G}_i\}) \tag{17}$$

where τ_f and $\tau_{\mathbf{G}}$ are relaxation times.

The form of the equations of motion and thermodynamic equilibrium follow from the choice of the moments of the equilibrium distributions f_i^{eq} and $\mathbf{G}_i^{eq}$ and the driving terms p_i and $\mathbf{M}_i$. These

quantities must obey the following constraints [22–24]:

$$\sum_i f_i^{eq} = \rho, \quad \sum_i f_i^{eq} e_{i\alpha} = \rho u_\alpha,$$

$$\sum_i f_i^{eq} e_{i\alpha} e_{i\beta} = -\Pi_{\alpha\beta} - \Pi_{\beta\alpha} + \rho u_\alpha u_\beta \tag{18}$$

$$\sum_i p_i = 0, \quad \sum_i p_i e_{i\alpha} = \partial_\beta(\Pi_{\alpha\beta} - \Pi_{\beta\alpha}), \quad \sum_i p_i e_{i\alpha} e_{i\beta} = 0 \tag{19}$$

$$\sum_i \mathbf{G}_i^{eq} = \mathbf{Q}, \quad \sum_i \mathbf{G}_i^{eq} e_{i\alpha} = \mathbf{Q} u_\alpha, \quad \sum_i \mathbf{G}_i^{eq} e_{i\alpha} e_{i\beta} = \mathbf{Q} u_\alpha u_\beta \tag{20}$$

$$\sum_i \mathbf{M}_i = \Gamma \mathbf{H}(\mathbf{Q}) + \mathbf{S}(\mathbf{W}, \mathbf{Q}), \quad \sum_i \mathbf{M}_i e_{i\alpha} = \left(\sum_i \mathbf{M}_i \right) u_\alpha \tag{21}$$

Conditions (18)–(21) are satisfied, as is usual in lattice Boltzmann schemes, by writing the equilibrium distribution functions and forcing terms as polynomial expansions in the velocity. The coefficients in this expansion are determined by evaluating the constraints Eqs. (18)–(21) and matching terms. They are given explicitly in Ref. [23]. Note than an alternative lattice Boltzmann scheme was recently proposed by Care *et al*. [25].

III. RESULTS

In this section we first study the viscous properties of a cholesteric liquid crystal subject to permeative flow and compare them with the ones found when the helix is perpendicular to the flow direction. We then compare the hydrodynamic double twist appearing for strong forcing to the static double twist found in blue phases. To this aim, we equilibrate and analyse the director profiles and defect structures of two different blue phases (BP I and BP II).

In the simulations presented below a cholesteric pitch was discretised into 64 lattice points. Typically, 10^6 iterations were performed.

A. Permeative Flows and Shear Thinning in Cholesterics

We consider a cholesteric liquid crystal which is sandwiched between two plates at a distance L apart along the z-axis. In the permeation mode, the axis of the cholesteric helix lies in a direction parallel to the plates which we shall take as the y-axis. For comparison, we will also consider the alternative case in which the helix lies along the z direction. The primary flow is imposed along the y-axis via a pressure gradient. Note that the modelling must be fully three-dimensional as, in general, a secondary flow takes place along x, i.e. the vorticity

direction. The elastic constant is $\sim$14.2 pN, which corresponds to the three Frank elastic constants [1,2] (splay, bend and twist) being all equal to $\sim$7.1 pN. The system size L is 3.4 μm and the equilibrium pitch of the cholesteric is 2.4 μm. The ratio between the two Leslie viscosities α_3 and α_2 [1,2] is $\alpha_3/\alpha_2 \sim 0.08$ so the liquid crystal is flow aligning, and the rotational viscosity is 1 Poise. Moreover at walls, no-slip velocity boundary conditions is considered and the helical texture is fixed.

Figure 1 shows the apparent viscosity as a function of the dimensionless ratio $\Delta pL^2/\eta c$ denoting the strength of forcing, where Δp is the applied pressure gradient, c is the speed of sound and η was defined below Eq. 8. The solid line refers to the permeation mode. For comparison we show also the analogous curve obtained when the helix axis lies perpendicular to the flow, i.e. along the z direction. It can be seen that for small forcing the apparent viscosity of the cholesteric liquid crystal in the permeation mode is more than one order of magnitude bigger ($\sim$30 times) than the typical isotropic viscosity obtained by switching the back-flow off. This very large increase is

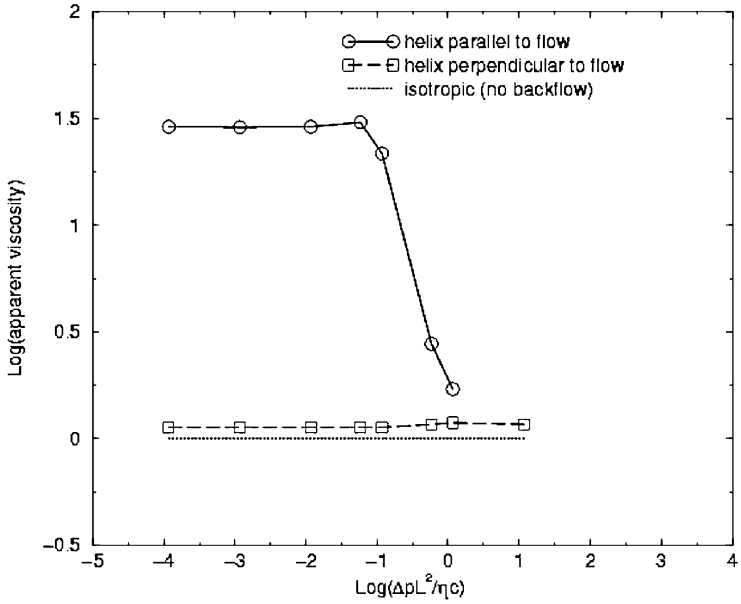

FIGURE 1 Apparent viscosity as a function of the dimensionless number $\Delta pL^2/\eta c$ characterising the strength of the forcing. The system size is 3.4 μm in all cases, and the cholesteric pitch is 2.4 μm.

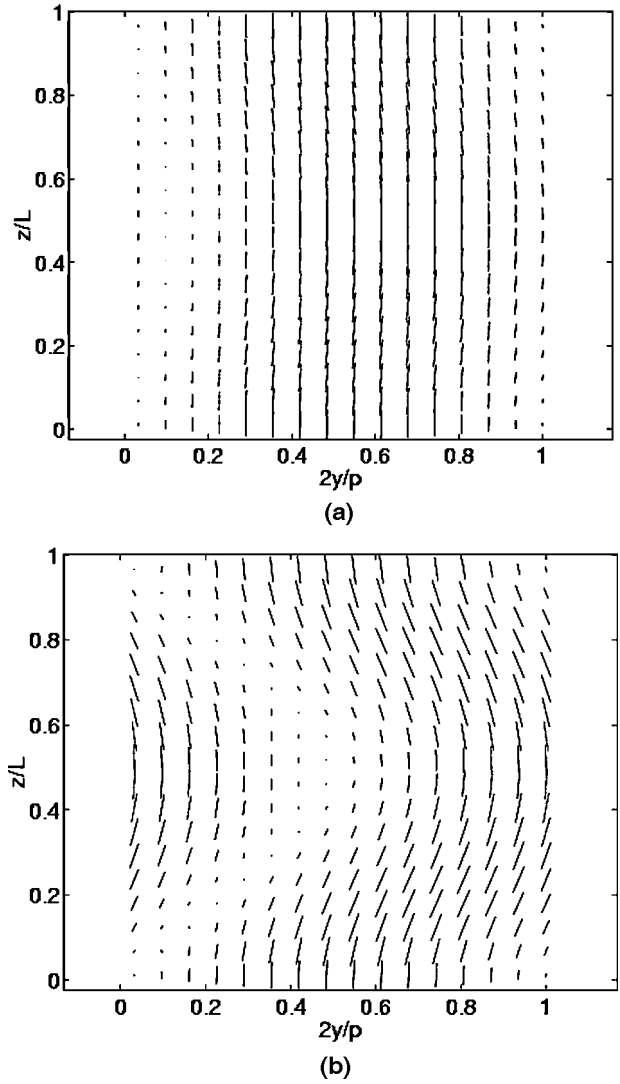

FIGURE 2 Director field profiles for (a) $\Delta pL^2/\eta c = 0.012$, the steady state is a 'chevron' and (b) $\Delta pL^2/\eta c = 0.06$, the steady state is doubly twisted.

due to the elastic energy which disfavours deformations of the original layered structure [26].

For very large forcing the original layered structure is destroyed and we observe a strong shear thinning behaviour (see Fig. 1). We also find evidence of shear thickening close to the rupture point. This

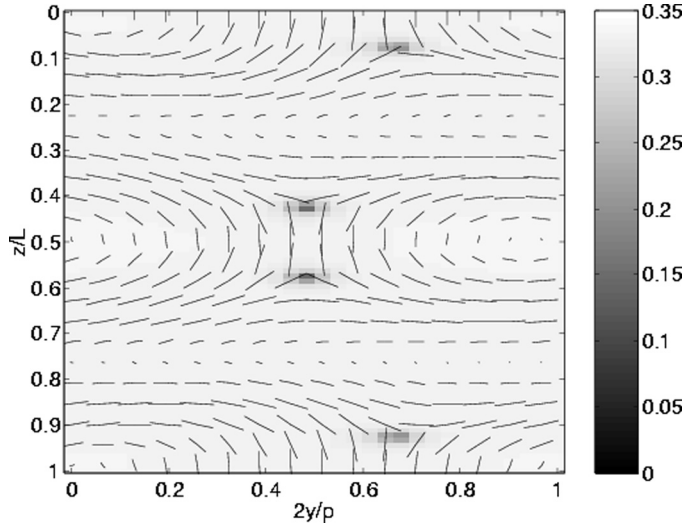

FIGURE 3 Director profile for a configuration characterised by double twist and disclinations in the steady state. Bright and dark regions correspond respectively to large and small values of the largest eigenvalue of the **Q** tensor.

is found both when the cholesteric helix is parallel and when it is perpendicular to the flow direction. The qualitative shapes of the viscosity versus forcing curves are in good agreement with experiments [18].

We now consider the deformations of the helical original texture caused by the flow. For small flows, the cholesteric layers are slightly bent by the flow into a chevron structure (Fig. 2(a)). The amount of bending is dictated by the applied Δp. As the forcing is increased the chevrons become more bent until a threshold is achieved at which a new structure appears. This structure, shown in Figure 2(b), has a flow-induced twist in the z-direction. The period of the twist along z is roughly equal to the natural twist of the cholesteric liquid crystal. For stronger forcing we have also sometimes found a steady state solution in which the director organises into an array of doubly twisted cylinders along the x direction, separated by defects (see Fig. 3 for an example). Although it is more correct to speak of a crossover than an abrupt transition, we can identify the region of appearance of double twist as the end of the viscosity plateau in Figure 1. For still larger forcing, those for which the viscosity is comparable to that of an isotropic fluid, the initial structure is completely disrupted.

B. Equilibrium Properties of Cubic Blue Phases: A Comparison between Static and Dynamic Double Twist

Here we report the defect structure and director profiles of two observed blue phases, namely BP I and BP II, calculated numerically, in order to compare the textures characterising their equilibrium configurations with the doubly twisted textures found above. These are often referred to as O_8^- and O_2 respectively, according to the symmetry group by which they are characterised.

Since we want to compute the defect structure associated with the cubic blue phases after equilibration, we need to apply our lattice Boltzmann algorithm to solve Eq. 5 starting from a suitable initial condition. In this work we take as initial conditions the analytical expressions given in Ref. [7], which are valid in the 'infinite chirality' limit. In our case this limit corresponds to setting $A_0 = 0$ so that the free energy is only given by the distortion part.

We choose $A_0 = 0.01$ and $\gamma = 3$, while the elastic constant is $K = 0.01$ for BP II, and $K = 0.005$ for BP I (simulation units). Blue phases are often characterised via their chirality κ and reduced temperature τ (defined in Ref. [11]). Our parameters correspond to $\kappa = 0.59$ and $\tau = 0.35$. The resulting disclination line networks are shown in Figure 4. The tubes represent regions of the blue phase unit cell in which the order parameter drops below some specified threshold, i.e. they represent disclination lines. The thickness of the tubes is related to the width of the defect cores.

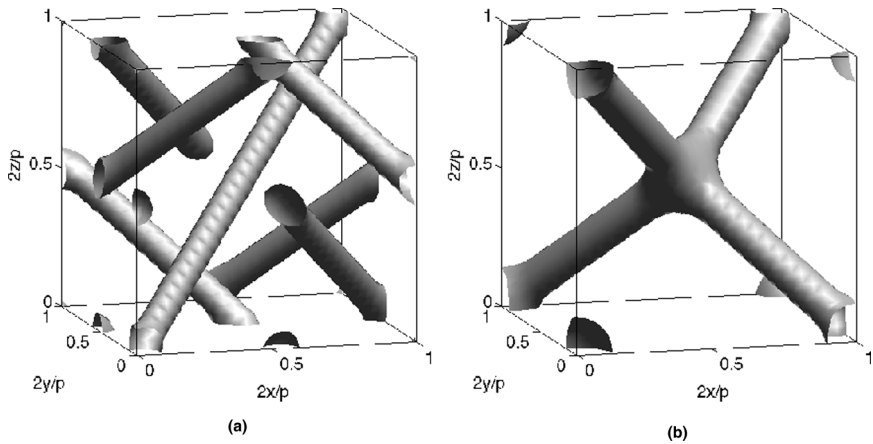

FIGURE 4 Disclination line networks characterising BP I (left) and BP II (right). The 'pitch' p used to scale the axis is – analogously to the case of the helical phase – half the periodicity of the unit cell in the corresponding blue phase.

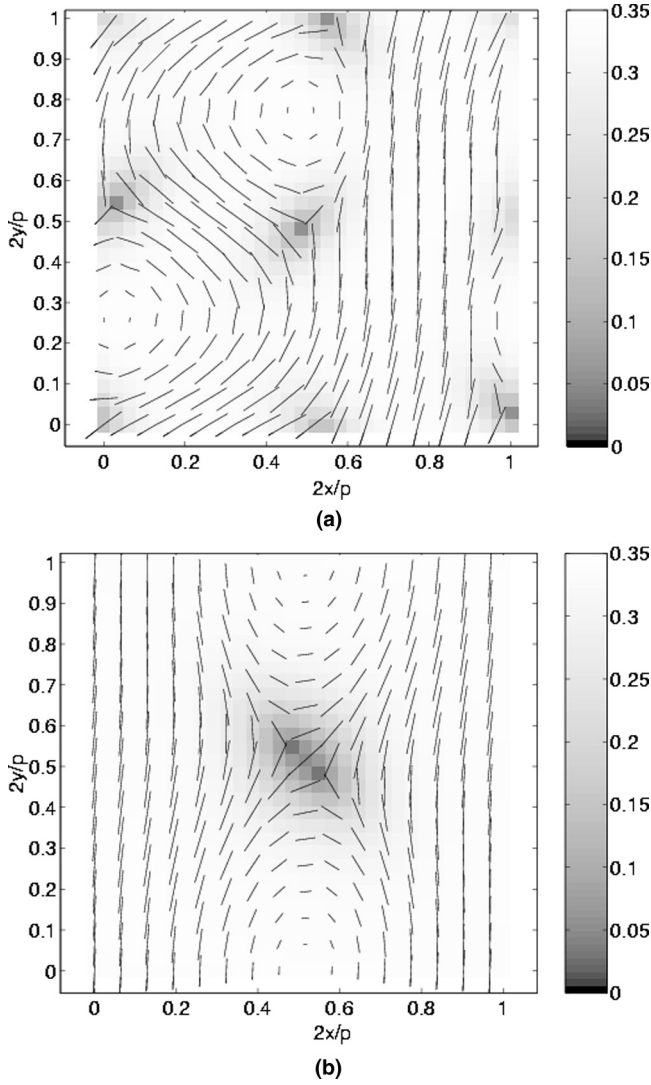

FIGURE 5 Director profiles at $z = L/2$ for BP I (left) and BP II (right). Bright and dark regions correspond to large and small values of the largest eigenvalue of the **Q** tensor.

These structures are in good agreement with those obtained in Refs. [11,12]. We note that the structure of the defects depends on the parameters. If A_0 or γ are increased, then the width of the disclinations decreases. We find that in the case of BP I the disclination line

network of the equilibrated structure is much better defined that the one characterising the infinite chirality solution, in which the tubes are not well defined.

It is known from the literature that the disclination line network is due to the frustration inherent in trying to patch together different regions of double twist. It is interesting to study the director profile of our equilibrated configurations to highlight this. In Figure 5 we show the director profiles in a plane parallel to the xy plane at $z = L/2$. It is apparent that the disclination structure is connected to the double twist. The texture characterising especially BP II is most similar to the doubly twisted texture obtained dynamically when a cholesteric helix flows in the permeative mode (see Fig. 3).

IV. CONCLUSIONS

We have presented a lattice Boltzmann algorithm which allows us to solve the Beris-Edwards equations of motion for cholesteric liquid crystals. We have given details of the algorithm and applied it to study permeative flows in cholesteric liquid crystals in which the helical texture was fixed at the boundaries. We found that the viscoelastic behaviour of the liquid crystal is characterised by a large apparent viscosity and by strong shear thinning. We also characterised the director field deformation induced by the flow. For small forcing, the cholesteric layers bend into chevrons. As the forcing is increased, we identify a flow-induced double twist along the velocity gradient direction. We have finally equilibrated two structures corresponding to blue phase I and II, in which double twist characterises the *static* director profile, and shown the similarity between the two configurations. This suggests that the lattice Boltzmann algorithm may also be used to characterise the equilibrium states and investigate the rheological properties of blue phases.

REFERENCES

[1] de Gennes, P. G. & Prost, J. (1993). *The Physics of Liquid Crystals*, 2nd Ed. Clarendon Press: Oxford.
[2] Chandrasekhar, S. (1980). *Liquid Crystals*, Cambridge University Press.
[3] Livolant, F. (1987). *J Phys.-Paris*, *48*, 1051.
[4] Strey, H. H., Wang, J., Podgornik, R. *et al.* (2000). *Phys. Rev. Lett.*, *84*, 3105.
[5] Grelet, E. & Fraden, S. (2003). *Phys. Rev. Lett.*, *90*, 198302.
[6] Roberts, N. W., Guillou, J. P. S., & Gleeson, H. F. (2004). *Mol. Cryst. Liq. Cryst.*, *411*, 1099; Raynes, E. P., Brown, C. V., & Stromer, J. F. (2003). *Appl. Phys. Lett.*, *82*, 13.
[7] Wright, D. C. & Mermin, N. D. (1989). *Rev. Mod. Phys.*, *61*, 385.

[8] Marcus, M. & Goodby, J. W. (1982). *Mol. Cryst. Liq. Cryst. Lett.*, *72*, 297.
[9] Cao, W. Y., Munoz, A., Palffy-Murohay, P. *et al.* (2002). *Nat. Mater.*, *1*, 111.
[10] Kikuchi, H., Yokota, M., Hisakado, Y. *et al.* (2002). *Nat. Mater.*, *1*, 64.
[11] Grebel, H., Hornreich, R. M., & Shtrikman, S. (1984). *Phys. Rev. A*, *30*, 3264.
[12] Meiboom, S., Sammon, M., & Berreman, D. W. (1983). *Phys. Rev. A*, *28*, 3553.
[13] Meiboom, S., Sethna, J. P., Anderson, P. W., & Brinkman, W. F. (1981). *Phys. Rev. Lett.*, *46*, 1216.
[14] Helfrich, W. (1969). *Phys. Rev. Lett.*, *23*, 372; Lubensky, T. C. (1969). *Phys. Rev.*, A, *6*, 452.
[15] Porter, R. S., Barrall, E. M., & Johnson, J. F. (1966). *J. Chem. Phys.*, *45*, 1452.
[16] Scaramuzza, N., Simoni, F., & Bartolino, R. (1984). *Phys. Rev. Lett.*, *53*, 2246.
[17] Hongladarom, K., Secakusuma, V., & Burghardt, W. R. (1994). *J Rheol.*, *38*, 1505.
[18] Ramos, L., Zapotocky, M., Lubensky, T. C., & Weitz, D. A. (2002). *Phys. Rev. E*, *66*, 031711.
[19] Rey, A. D. (2002). *J. Rheol.*, *46*, 225; (2000). *J. Rheol.*, *44*, 855.
[20] Prost, J., Pomeau, Y., & Guyon, E. (1991). *J. Phys. II*, *1*, 289.
[21] Beris, A. N. & Edwards, B. J. (1994). *Thermodynamics of Flowing Systems*, Oxford University Press: Oxford.
[22] Denniston, C., Orlandini, E., & Yeomans, J. M. (2001). *Europhys. Lett.*, *52*, 481; (2001). *Phys. Rev. E*, *63*, 056702.
[23] Denniston, C., Marenduzzo, D., Orlandini, E., & Yeomans, J. M. (2004). *Phil. Trans. R. Soc. Lond. A*, *362*, 1745.
[24] Chen, S. & Doolen, G. D. (1998). *Annu. Rev. Fluid Mech.*, *30*, 329.
[25] Care, C. M., Halliday, I., Good, K., & Lishchuk, S. V. (2003). *Phys. Rev. E*, *67*, 061703.
[26] Marenduzzo, D., Orlandini, E., & Yeomans, J. M. (2004). *Phys. Rev. Lett.*, *92*, 188301.